Available online at www.sciencedirect.com
ScienceDirect
International Journal of Solids and Structures 45 (2008) 3779–3792
INTERNATIONAL JOURNAL OF SOLIDS AND STRUCTURES
www.elsevier.com/locate/ijsolstr

Peeling experiments of ductile thin films along ceramic substrates – Critical assessment of analytical models

Yueguang Wei *, Haifeng Zhao

LNM, Institute of Mechanics, Chinese Academy of Sciences, Beijing 100080, PR China

Received 27 May 2007; received in revised form 19 October 2007
Available online 4 November 2007

Abstract

Two types of peeling experiments are performed in the present research. One is for the Al film/Al_2O_3 substrate system with an adhesive layer between the film and the substrate. The other one is for the Cu film/Al_2O_3 substrate system without adhesive layer between the film and the substrate, and the Cu films are electroplated onto the Al_2O_3 substrates. For the case with adhesive layer, two kinds of adhesives are selected, which are all the mixtures of epoxy and polyimide with mass ratios 1:1.5 and 1:1, respectively. The relationships between energy release rate, the film thickness and the adhesive layer thickness are measured during the steady-state peeling process. The effects of the adhesive layer on the energy release rate are analyzed. Using the experimental results, several analytical criteria for the steady-state peeling based on the bending model and on the two-dimensional finite element analysis model are critically assessed. Through assessment of analytical models, we find that the cohesive zone criterion based on the beam bend model is suitable for a weak interface strength case and it describes a macroscale fracture process zone case, while the two-dimensional finite element model is effective to both the strong interface and weak interface, and it describes a small-scale fracture process zone case.

Keywords: Peel experiment; Metal thin film; Analytical model; Interfacial fracture energy

1. Introduction

Researches on the interface properties have been attracting a great deal of interest in last several decades. Interface, between one material with other material, film with substrate, metal with ceramic, soft material with hard material, biomaterial with engineering material, etc., covers a wide research subjects and applications, and it plays an important role in materials protecting, connecting, strengthening, or toughening etc.. The measurements of interface mechanical properties, such as the measurements of adhesion strength and adhesion energy, etc., are significant to optimize and design a high-quality interface. Peel test is one of the most important methods to measure the interface mechanical properties, mainly for measuring the interface properties between films and substrates. It is a simple test method, was designed and presented 50 years ago by Spies

* Corresponding author. Tel.: +86 1062648721; Fax: +86 1062561284.
E-mail address: ywei@LNM.imech.ac.cn (Y. Wei).

0020-7683/$ - see front matter © 2007 Elsevier Ltd. All rights reserved.
doi:10.1016/j.ijsolstr.2007.10.023

(1953). Due to simplicity, the peel test has been widely applied in many research areas (Leseman et al., 2007; Williams and Kauzlarich, 2006, 2005; Fedorov and De Hosson, 2005; Kawashita et al., 2005; Johnson and Kauzarich, 2004; Moody et al., 2003; Wei, 2002; Wei et al., 2002; Feliu-Baez et al., 2001; Choi and Oh, 2001; Asai et al., 2001; Bundy et al., 2000; Kawabe et al., 2000). Specifically, when both the thin film and the substrate are elastic materials, the interfacial adhesion properties (such as adhesion strength and toughness, etc.) can be obtained directly by measuring the peel force per unit width of film which is equal to the energy release rate (ERR) of system. Actually, under steady-state peeling the energy release rate of system is equal to the interfacial adhesion energy (per unit area) from energy balance. However, when the thin film is a ductile material, the measured ERR is often much larger than the interfacial adhesion energy since plastic dissipation occurs within the film. The plastic dissipation makes the exerted ERR increase considerably to maintain the thin film delaminating. In order to model the ERR when plastic dissipation occurs, Kim and his coworkers (Kim and Aravas, 1988; Kim and Kim, 1988; Kim et al., 1989) presented a plastic bending model to predict the plastic dissipation of ductile thin films. In the decade or more following that with most analyses on ductile thin film peeling adopted or referred to this bending model (Kinloch et al., 1994; Thouless et al., 1997; Moidu et al., 1998; Park and Yu, 1998; Yang et al., 1999). Wei and Hutchinson (1998) adopted a different method to analyze elastic–plastic film peeling process. In Wei and Hutchinson's analysis, the thin film steady-state peeling process was simulated by using the two-dimensional (2D) plane-strain elastic–plastic finite element (FE) method, except for the detached part of thin film which was still described by the bending model. They obtained different results from that based on the bending model qualitatively and quantitatively. An important question is thus: what model is the most reliable? Considering that the bending model is simple and can be easily used to interpret applications, one wants to know the condition under which the bending model result is reliable.

Considering that the peel test is widely applied and plays an important role in thin film engineering, it is very important and necessary to clear up that point. For this purpose, several experts (Cotterell et al., 2002; 2003) proposed a round robin on the analysis of the peel test involving a comparison research on Kim model and Wei–Hutchinson model.

Usually, a complete characterization on an elastic–plastic crack growth process requires a double-parameter criterion (Rice, 1974; Betegon and Hancock, 1991; Suo et al., 1993; Tvergaard and Hutchinson, 1993; Wei and Wang, 1995a,b). Since the peeling process of the ductile thin film is an elastic–plastic interfacial separation (fracture) process, double-parameter criterion is thus needed to characterize the process. Wei (2004) presented three double-parameter criteria based on the bending model and used them to analyze the nonlinear peeling of the ductile films in detail. In Wei's studies, bending model predictions based on three double-parameter criteria were compared with the 2D plane-strain FE model predictions, and some connection between two kinds of model solutions was presented.

Although the peel test bending models were checked by FE simulations in Wei (2004), the effectiveness and effective scopes of all analytical models are still unclear and need to be checked using a systematic peel experiments. Modeling results need to compare with experimental results in detail. Therefore, in the present research, a series of peeling experiments for Al and Cu films bonded on the ceramic substrate with and without an adhesive layer will be performed. The relations of steady-state energy release rate with film thickness will be measured. The effectiveness of analytical models will be assessed through comparing modeling and present experimental results. Some connections of analytical models will be discussed in detail.

2. Overview of modeling results for peel test

2.1. Elastic–plastic peeling problem

Steady-state peeling process of an elastic–plastic thin film is described in Fig. 1. Under the action of an external force P per unit width of film, thin film undergoes delamination, plastic loading and unloading. Segments OA, AB and BD in the graph of Fig. 1 are referred to the elastic bending, elastic–plastic bending as well as the unloading bending, respectively. DE is referred to the reverse plastic bending. State E shows that the portion of thin film is pulled into straight line and the corresponding film curvature is zero. The section EF is the second unloading state.

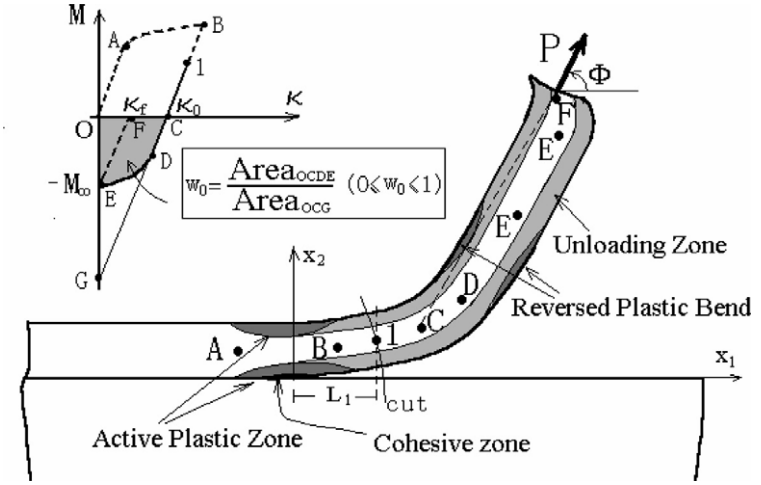

Fig. 1. Deformation and simplified model for thin film nonlinear peeling process.

Under steady-state peeling condition, the ERR of the system, $P(1-\cos\Phi)$, can be expressed as follows from energy balance:

$$P(1-\cos\Phi) = \Gamma_0 \tag{1}$$

for elastic peeling process, and

$$P(1-\cos\Phi) = \Gamma_0 + \Gamma^{\mathrm{P}} \tag{2}$$

for elastic–plastic peeling process, where Γ_0 is the interfacial fracture energy (toughness), Γ^{P} is the plastic dissipation, Φ is peeling angle. In the peel test study for ductile film case, to determine Γ^{P} is the most important task. So one can further determine the interfacial fracture energy Γ_0.

2.2. The results based on the criteria of beam bending model

Based on the bend model, Wei (2004) derived the detailed relation between moment and curvature, and the expressions of Γ^{P} for three double-parameter criteria, respectively.

The thin film peeling process and delamination can be characterized by the double-parameter criterion (a single-parameter criterion is for an elastic delamination). Three double-parameter criteria, which are sketched in Fig. 2, were used previously to describe the elastic–plastic peeling process (Wei, 2004). Fig. 2(b) is the conventional cohesive zone model, which has two independent parameters, $(\Gamma_0, \hat{\sigma})$, where Γ_0 is interfacial fracture toughness, or adhesion energy per unit area, $\hat{\sigma}$ is the interfacial separation strength. Fig. 2(c) is a model taking Γ_0 and the crack tip critical slope angle $\theta^{\mathrm{c}}_{\mathrm{tip}}$ as the governing parameters. This characterization was first adopted by Kim and his coworkers (see Kim and Aravas, 1988; Kim and Kim, 1988; Kim et al., 1989). Fig. 2(d) is a model based on two parameters$(\Gamma_0, \bar{\varepsilon}_{\mathrm{c}})$ adopted by Wei (2004), where $\bar{\varepsilon}_{\mathrm{c}}$ is the critical value of Mises effective strain for thin film at the crack tip. Combining these two independent parameters and the relationship of the elastic–plastic bending, Wei (2004) derived and obtained the solutions for the elastic–plastic peeling process. The representative results are summarized in Fig. 3(a), where a length scale parameter R_0 is introduced in the solutions, which is defined as follows

$$R_0 = \frac{E\Gamma_0}{3\pi(1-\nu^2)\sigma_{\mathrm{Y}}^2} \tag{3}$$

and characterizes the plastic zone size in the film in the small scale yielding, E is Young's modulus of film, ν is Poisson's ratio, σ_{Y} is yield strength, $\varepsilon_{\mathrm{Y}} = \sigma_{\mathrm{Y}}/E$, N is strain hardening exponent in the solutions. In Fig. 3(a), the variations of the normalized ERR with the normalized thin film thickness based on the double-parameter criteria $(\Gamma_0, \hat{\sigma})$ (cohesive zone model), $(\Gamma_0, \theta^{\mathrm{c}}_{\mathrm{tip}})$ and $(\Gamma_0, \bar{\varepsilon}_{\mathrm{c}})$ are plotted, respectively. Because of that in the

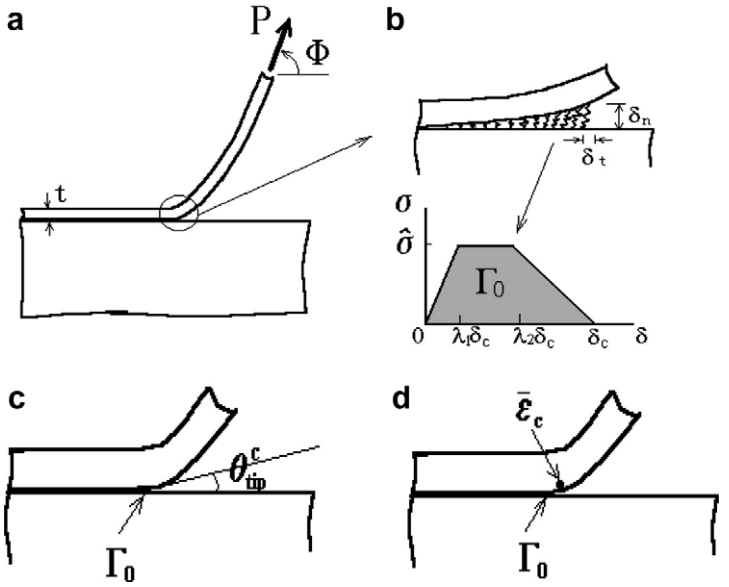

Fig. 2. Three double-parameter criteria for peeling test. (a) Peel test geometry, (b) $(\Gamma_0, \hat{\sigma})$ criterion, (c) $(\Gamma_0, \theta^c_{tip})$ criterion, (d) $(\Gamma_0, \bar{\varepsilon}_c)$ criterion.

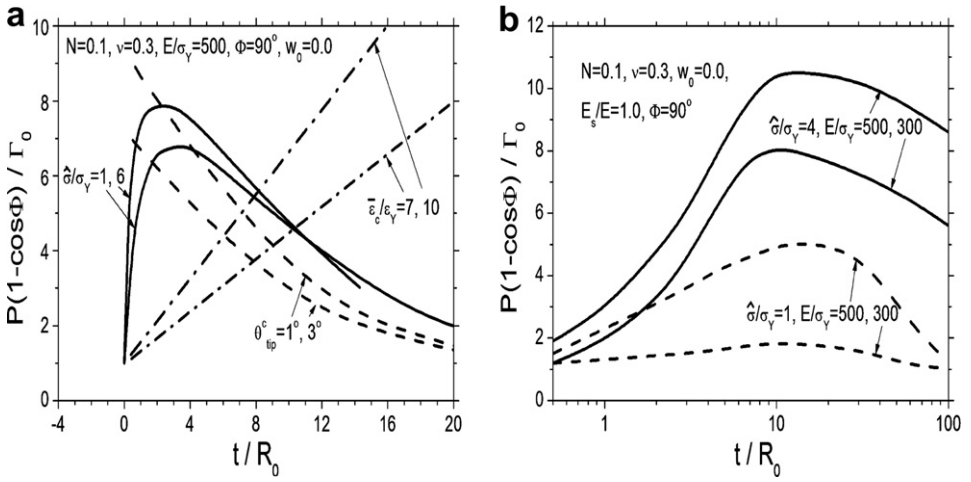

Fig. 3. Modeling results: variations of the normalized energy release rates with film thickness based on three double-parameter criteria of bend model (a) and cohesive zone criterion of the 2D FE model (b).

elastic peeling case, $P(1-\cos\Phi)/\Gamma_0 = 1$, evidently, the value of the normalized ERR under elastic–plastic peeling is remarkably enlarged by the plastic dissipation. If the plastic dissipation is small or can be neglected, the normalized ERR tends to unity. For the $(\Gamma_0, \hat{\sigma})$ criterion, starting at $t/R_0 \approx 0$, as film thickness increases, the normalized ERR, $P(1-\cos\Phi)/\Gamma_0$ increases sharply and reaches a maximum value at about $t/R_0 = 2$, and after $t/R_0 = 2$, the normalized ERR decreases and gradually tends to unity with increasing the film thickness. Surprisingly, for the $(\Gamma_0, \hat{\sigma})$ criterion, the normalized ERR is relatively insensitive to the interface separation strength, $\hat{\sigma}/\sigma_Y$, unlike conventional fracture analyses (Tvergaard and Hutchinson, 1993; Wei and Hutchinson, 1997a,b). For the $(\Gamma_0, \theta^c_{tip})$ criterion, the variation of $P(1-\cos\Phi)/\Gamma_0$ as a function of t/R_0 is different from that based on the criterion $(\Gamma_0, \hat{\sigma})$, decreases monotonically as film thickness increases. The smaller the film thickness, the larger the normalized energy release rate. This feature is consistent with that given by Kim and his collaborators for incompressible material (Kim and Aravas, 1988; Kim and Kim, 1988; Kim et al., 1989). For

the $(\Gamma_0, \bar{\varepsilon}_c)$criterion, another feature is displayed: $P(1-\cos\Phi)/\Gamma_0$ increases linearly with increasing t/R_0. The slopes of the straight lines increase with increasing $\bar{\varepsilon}_c$. However, partial solutions corresponding to $\theta_{tip} < 0$ should be cut off when either $\bar{\varepsilon}_c$ or t/R_0 is too large (Wei, 2004).

2.3. The results based on 2D plane-strain FE analysis model

The cohesive zone model was adopted here, and the governing parameters were still selected as $(\Gamma_0, \hat{\sigma})$ (Wei and Hutchinson, 1998; Wei, 2004).

Two-dimensional elastic–plastic finite element analysis model was adopted by Wei and Hutchinson (1998) and Wei (2004). This method can be delineated briefly here. Referring to Fig. 1, the detached portion on the right hand side of cross-section 1 is treated with the bending model, while the deformations of other portions including thin film on the left side of cross-section 1 and substrate are treated with the finite element simulation. The bending model solution for the detached portion on the right side of cross-section 1 is applied on the cross-section 1 when the second problem is simulated by using the finite element method. The corresponding results for the normalized ERR have already been presented by Wei (2004). The representative results are summarized here in Fig. 3(b). From Fig. 3(b), obviously, the normalized ERR is very sensitive to the values of $\hat{\sigma}/\sigma_Y$ and E/σ_Y. For a strong interface adhesion case, $\hat{\sigma}/\sigma_Y = 4$, when film thickness is very large, i.e., for $t/R_0 > 15$, the normalized ERR slowly decreases with increasing t/R_0. However, for a weak interface adhesion case, $\hat{\sigma}/\sigma_Y = 1$, and for $t/R_0 < 12$, the normalized ERR increases as t/R_0 increases first, then tends to a maximum value. For $t/R_0 > 15$, increasing t/R_0 further decreases the normalized ERR to tend to unity for very large film thickness.

3. Peeling experiments

In order to check effectiveness of above analytical models for peel test, two types of the peeling experiments are performed here. One type of the peeling experiments is for Al film peeled along Al_2O_3 substrate with an adhesive layer between film and substrate. A series of film thicknesses are selected in the experiments. Another type of the peeling experiments is for the super-thin Cu films peeled along Al_2O_3 substrate without the adhesive layer between film and substrate. The film thickness is at the micron level.

3.1. Film/substrate system with an adhesive layer

A series of peel experiments are performed to investigate the effects of the film thickness, peel angle and adhesive layer thickness on total energy release rate of system.

3.1.1. Experimental procedure review

Peel experiments are performed for a series of the Al film thicknesses, 20, 50, 80, 100, 200, 225 and 250 microns, bonded to the 4.5 mm thick Al_2O_3 substrates with two types of epoxy/polyimide adhesives with 20 micron thickness. Two kinds of mass ratios of epoxy to polyimide in the adhesives, 1:1 and 1:1.5, are adopted respectively. The first kind of the adhesive (mass ratio is 1:1) shows a fragile property in the peel tests and the second kind of the adhesive (mass ratio is 1:1.5) shows ductile property. Additionally, in order to check the effect of the adhesive layer, a series of adhesive layer thicknesses are considered for two kinds of adhesives, respectively, in the peeling experiments when film thickness is fixed.

It is a crucial thing to control the adhesive layer thickness w in preparing the samples. In our peel tests the adhesive layer thickness is kept constant by adding a small quantity of the SiO_2 spheres into the adhesive (see Fig. 4).

Peel experiments are performed using a standard tensile testing machine with a small-scale peel test rig made specifically for the peel test (see Fig. 5). A constant peel angle can be easily maintained during experiment with the rig. A Questar Measuring Microscope with long focus is used to observe the crack growth and to take photos. It is difficult that the thin film is fixed to the testing machine directly, so in order to protect the films from tearing, a piece of adhesive tape is used to connect the film to some small metal sheet, and then a thin nylon thread is used to connect the metal sheet to the testing machine. Since the nylon thread is one meter

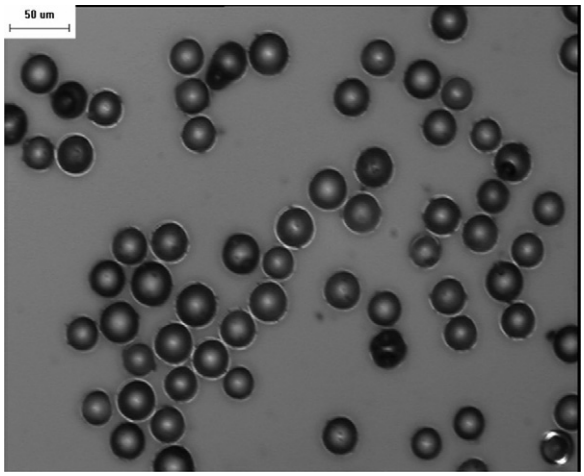

Fig. 4. Photo of mixed adhesive with epoxy/polyimide and a small percentage of SiO_2 particles.

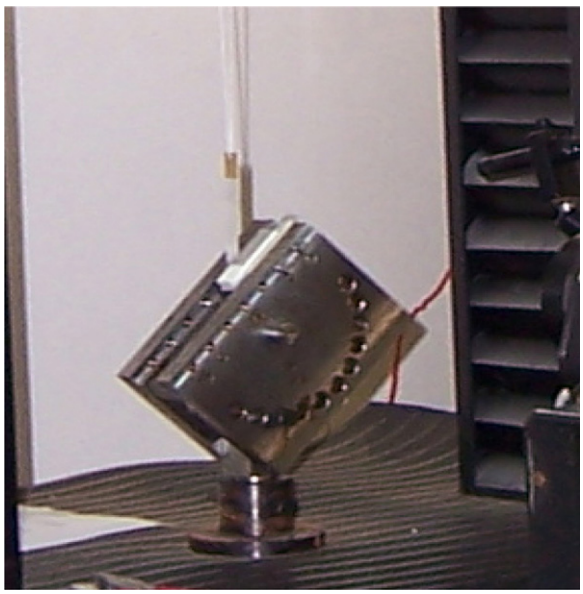

Fig. 5. Peel test rig made specially for adjusting peel angle.

long and the crosshead displacement is not more than 30 mm, the change of the peel angle during experiment is not over 1.5°, so the peel angle is kept approximately.

Stress–strain relations of the adhesives are measured experimentally through uniaxial tension tests, and the results are shown in Fig. 6(a) and (b) for a ductile adhesive and for a fragile adhesive, respectively. From Fig. 6, the stress–strain curves of both ductile and fragile adhesive materials display plastic softening. From Fig. 6(a) and (b), ductile adhesive displays the lower strength and much larger failure strain than that of fragile adhesive. The failure strain of the fragile adhesive is about 9%.

3.1.2. Peeling experimental results

The curves of peel force per unit width of film vs. crosshead displacement are recorded during the peeling experiments. Fig. 7(a) and (b) show the typical results for the ductile and fragile adhesive cases, respectively. From Fig. 7, the peel process can be divided into two stages: pre-peeling and steady-state peeling. The steady-

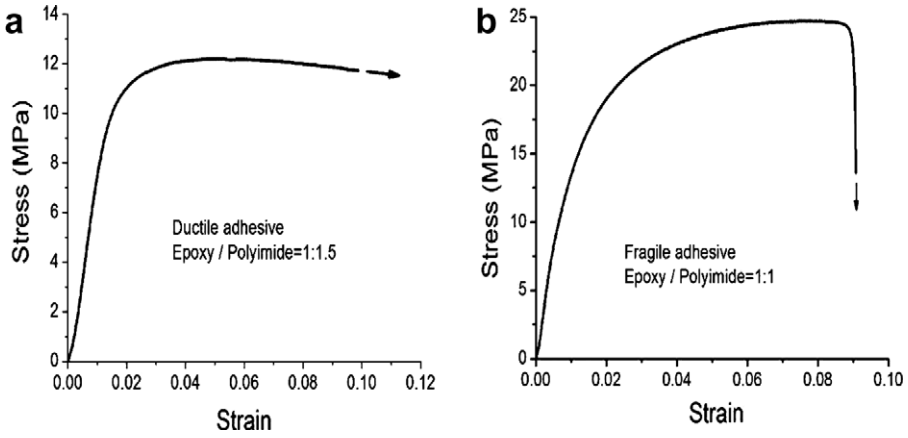

Fig. 6. Stress–strain curves of adhesives measured under unidirectional tension experiments.

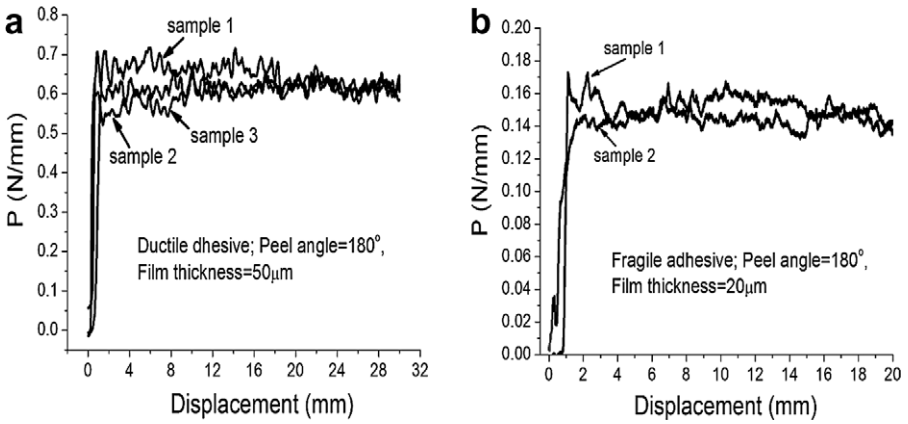

Fig. 7. Experimental results: typical curves of the peel force per unit width of film vs. crosshead displacement during peeling process. A steady-state peeling process is obtained easily. (a) For ductile adhesive case and (b) for fragile adhesive case.

state peeling is concerned here. Comparing the results shown in Fig. 7(a) and (b), the steady-state peel force per unit width of film (ERR) corresponding to the ductile adhesive (ratio is 1:1.5) is over four times that of the fragile adhesive case. So the ductile adhesive corresponds to a strong interface adhesion, while the fragile adhesive corresponds to a weak interface adhesion.

For comparison, at least three samples are used to do peel experiments for each case of film thickness and peel angle. The mean values of the measured steady-state peel forces per unit width of film (ERR) are plotted in Fig. 8 as the function of the film thickness for three typical peeling angles, $\Phi = 90°$, 135° and 180°. The measured ERR for the ductile adhesive case is obviously larger than that of the fragile adhesive case. For the ductile adhesive case, generally the ERR increases with increasing film thickness, however, for the fragile adhesive case there exists a maximum value point at the ERR curve, after that point the ERR value decreases with increasing film thickness. From Fig. 8, peeling angle (Φ) has a considerable influence on the ERR value. Combining the definition of the ERR, $P(1 - \cos\Phi)$, and the experimental results of peel force per unit width of film shown in Fig. 8, obviously, the ERR values increase with peeling angle monotonically, which implies that there is a larger plastic zone size near crack tip, corresponding to larger plastic dissipation during the peeling process in the case of $\Phi = 180°$ (or 135°) than that in the case of $\Phi = 90°$. The larger plastic dissipation will cause larger difficulty in the experimental measurements of interface properties. Therefore, peeling angle $\Phi = 90°$ would be the most appropriate one to use in the peel test, compared with other peeling angle case, such as $\Phi = 180°$ and 135°.

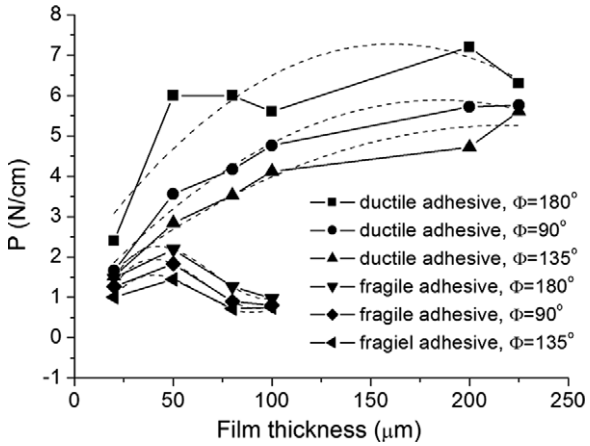

Fig. 8. Experimental results: variations of the ERR with film thickness are measured for both strong and weak interface adhesions and for three peel angles. In all cases, adhesive layer thickness is equal to 20 microns.

The effects of the adhesive layer thickness are also investigated experimentally. The ERR as the functions of the adhesive layer thickness is plotted in Fig. 9(a) and (b) for both ductile and fragile adhesives, respectively. The ERR increases with increasing film thickness, and tends to a stable value, which corresponds to the small scale yielding case of the film. From Fig. 9, the peeling angle has also a large influence on the ERR values.

3.2. Peeling experiments for super-thin film/substrate system without adhesive layer

According to our knowledge, until now the film thicknesses of most peeling experiments performed were larger than several tens of micron, and the film was bonded onto substrate with an adhesive layer, however, most analytical models for peeling problems did not include the adhesive layer. In the present research, we try to carry out a kind of peeling experiments for the film/substrate system without adhesive layer between film and substrate. In our experiments, Cu film was sputtered and electroplated onto the Al_2O_3 substrate. During the preparation of the film/substrate system, we found that it was very difficult to obtain a thick film/substrate system according to this method, so we obtained a super-thin film/substrate system with film thickness at the micron level.

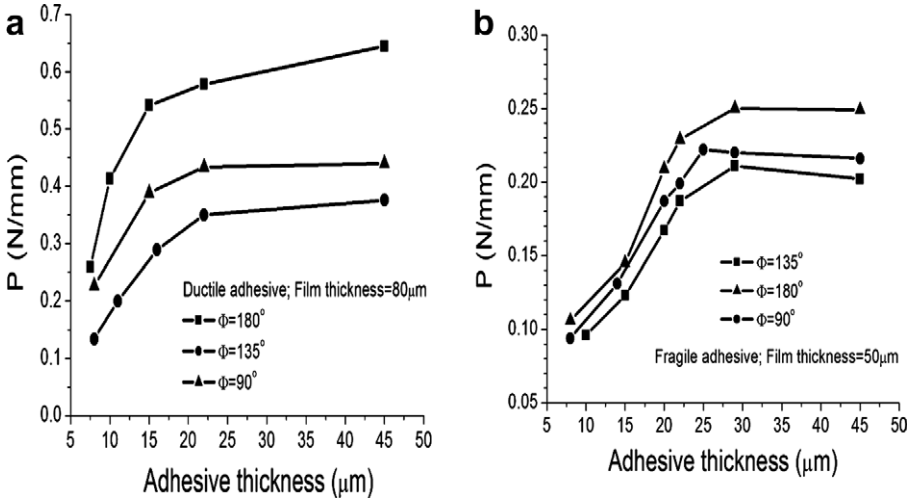

Fig. 9. Experimental results: variations of the ERR with adhesive layer thickness for both the ductile adhesive (a) and the fragile adhesive (b).

3.2.1. Experimental procedure review

A big piece of Al_2O_3 is cut to small cubic samples with size of 40 mm × 2 mm × 5 mm. The sample surfaces on which Cu film will be electroplated are polished, washed using ultrasonic and water, and then dried. After drying, Cu film is electroplated onto the polished surface. Noting that it is difficult to directly electroplate Cu film onto the Al_2O_3 substrates due to the poor conductance of Al_2O_3, we use a two-step technique to complete the process, first sputtering then electroplating. Since the sputtering process is very slow (i.e., maximum sputtering velocity is several nanometers of thickness per minute), in the present experiments, 500 nm thickness of films is sputtered and then the remainder thickness of the films is electroplated. Six kinds of specimens respectively with film thickness, 1, 2, 3, 5, 10 and 15 μm are made by using above process. Before sputtering, vacuum grease is coated on the right half region of each sample surfaces for making a 20 mm long pre-crack to facilitate the peel test operation.

All peel experiments are conducted on a standard tensile testing machine (also see Fig. 5). A minisize sensor with high precision is used to measure the peel force. The peel angle is kept at 90° and the crosshead velocity is kept at 0.2 mm/min during peel experiments.

3.2.2. Experimental results

During the peel experiments the peel force per unit width of film as a function of the crosshead displacement is recorded. Fig. 10(a)–(c) show the measured typical curves of the variations of the peel force per unit

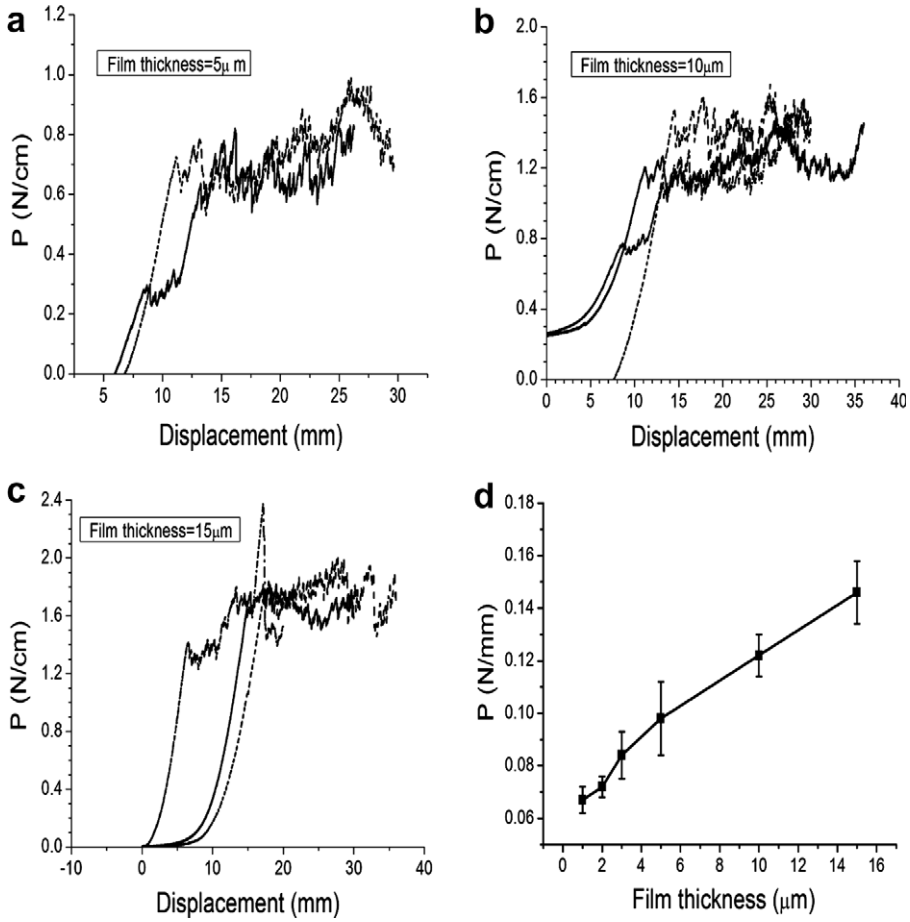

Fig. 10. Experimental results: typical curves of the peel force per unit width of film vs. crosshead displacement during peeling process for the super-thin film cases (a–c). The film is electroplated onto the substrate without adhesive layer between the film and the substrate. A steady-state process is obtained easily from figures. (d) is the variation of the ERR with the film thickness.

width of film with crosshead displacement for three cases of film thickness. The initial part of each curve corresponds to the elongation of the detached film. Then, crack initiates and propagates with exerting displacement. Finally the crack propagation (or film delamination process) tends to the steady-state process under keeping the external load fixed.

For each film thickness, three samples are used at least to do the peel experiments. The measured steady-state peel forces per unit width of film (ERR) are taken as the function of the film thickness, and are plotted in Fig. 10(d). Obviously, the ERR is proportional to the film thickness for the super-thin film case. The result seems to have a similar trend and to be consistent with that shown in Fig. 8 when film thickness is small. Using the results, the interface properties can be determined using an inverse analysis (Zhao and Wei, 2007).

4. Discussions through comparison of experimental and modeling results

4.1. On effects of adhesive layer thickness

Usual analytical models do not include adhesive layer along interface between metal film and ceramic substrate, as the adopted models shown in Fig. 2. The analytical results based on these models are shown in Fig. 3. However, specimens of most peeling experiments for the metal film/ceramic substrate system include an adhesive layer between film and substrate. This is because that when metal film thickness is larger than several tens of microns, one can easily make the film/substrate system through adopting an adhesive layer between film and substrate. Without the adhesive layer, it is very difficult to make such a system. Recently, the effects of the adhesive layer on the ERR were investigated by investigators (Andersson and Biel, 2006; Kawashita et al., 2005; Pardoen et al., 2005). For a film/substrate specimen with an adhesive layer, under the steady-state peeling experiment the ERR can be expressed according to energy balance (referring to Fig. 11a):

$$P(1-\cos\Phi) = \Gamma_0 + \Gamma_0' + \Gamma^{P'} \tag{4}$$

where Γ_0 is cohesive energy, Γ_0' is a dissipation energy in the adhesive layer, $\Gamma^{P'}$ is the plastic dissipation energy in the film. We can simply rewrite expression of Eq. (4) into the following form

$$P(1-\cos\Phi) = \bar{\Gamma}_0 + \Gamma^{P'} \tag{5}$$

where $\bar{\Gamma}_0 = \Gamma_0 + \Gamma_0'$. So under the steady-state peeling we can transfer the problem with an adhesive layer into another problem without the adhesive layer equivalently, as sketched in Fig. 11(b), through properly selecting two equivalent parameters $(\bar{\Gamma}_0, \hat{\bar{\sigma}})$. Therefore, the adhesive layer does not influence the solution trend of the energy release rate, and we can use the experimental results given in Figs. 8 and 9 to check the analytical model results shown in Fig. 3 from solution variation trends.

Furthermore, dissipation energy in the adhesive layer Γ_0' (see Fig. 11(a)) can be estimated using the following formula (referring to Wei and Hutchinson, 1997b)

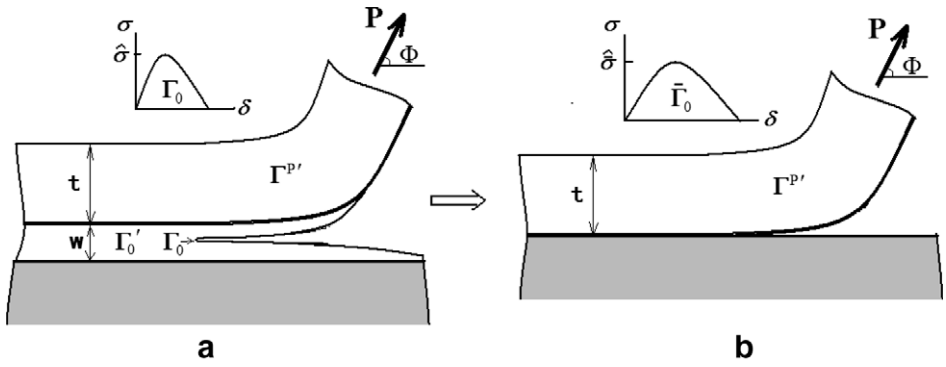

Fig. 11. Steady-state peeling for a film bonded to a substrate with an adhesive layer (a) is equivalent to a case without adhesive between the film and substrate (b).

$$\Gamma_0' = \int_0^w \left[\int_0^{\varepsilon_{ij}^{\mathrm{D}}} \sigma_{ij}\, \mathrm{d}\varepsilon_{ij} \right] \mathrm{d}y \tag{6}$$

where $\varepsilon_{ij}^{\mathrm{D}}$ is strain components at the downstream adhesive layer, w is adhesive layer thickness, integration "dy" is along the crosswise of adhesive layer at the downstream adhesive layer. As an example, let's consider the fragile adhesive case of the present research (see Fig. 6b). Assume that a full damage process takes place in the downstream adhesive layer under the steady-state peeling (noting that the assumption may be effective when adhesive layer thickness is small), so Γ_0' can be estimated approximately by

$$\Gamma_0' \approx wA_{\mathrm{c}} \tag{7}$$

whereA_{c} is area below the curve of stress–strain relation in Fig. 6(b), $A_{\mathrm{c}} = 1.78 \times 10^6\ \mathrm{N/m^2}$. Cohesive energy Γ_0 was determined by an inverse analysis (Zhao, 2007), 60 $\mathrm{J/m^2}$. Combining the experimental results shown in Fig. 9(b), thus, a comparison of the variations of P, Γ_0', Γ_0 and $\Gamma^{\mathrm{P}'}$ is given in Fig. 12. From Fig. 12, the plastic dissipation energy in film, $\Gamma^{\mathrm{P}'}$, is dependent on the equivalent interfacial fracture energy, $\bar{\Gamma}_0 = \Gamma_0 + \Gamma_0'$.

4.2. Effectiveness of analytical models

The peel test results based on three analytical criteria of $(\Gamma_0, \hat{\sigma})$, $(\Gamma_0, \theta_{\mathrm{tip}}^{\mathrm{c}})$ and $(\Gamma_0, \bar{\varepsilon}_{\mathrm{c}})$, under the beam bend model are shown in Fig. 3(a). Through comparing Fig. 3(a) of analytical model results with Fig. 8 of experimental results, one can find that there is a similar trend between modeling results based on the beam bend model using the criterion of $(\Gamma_0, \hat{\sigma})$ and experimental results for the fragile adhesive case (weak interface adhesion). Note that the analytical results based on the criterion of $(\Gamma_0, \theta_{\mathrm{tip}}^{\mathrm{c}})$ have a similar trend with the analytical results based on the criterion of $(\Gamma_0, \hat{\sigma})$ when film thickness t/R_0 is larger than 2. Through comparing Fig. 3(a) and experimental results shown in Fig. 8, one can also find that there is a similar trend between modeling results based on the beam bend model using the criterion of $(\Gamma_0, \bar{\varepsilon}_{\mathrm{c}})$ and experimental results when film thickness is small.

The analytical results based on the 2D elastic–plastic FE model are shown in Fig. 3(b) for higher strength interface and for lower strength interface, respectively. Through comparing these results with experimental results shown in Figs. 8 and 10(d), one can find that the analytical results for higher-strength interface and for lower-strength interface have the similar trends with experimental results for ductile adhesive and for fragile adhesive cases, respectively.

From above comparisons, we also note that the results based on the cohesive zone criterion for beam bend model and for the 2D FE model display the similar trend with experimental results for weak adhesive case. However, from Fig. 3(a) and (b) both kinds of results of analytical models have the different shapes and correspond to the different maximum value points of t/R_0. If one simulates the peeling experiments using the

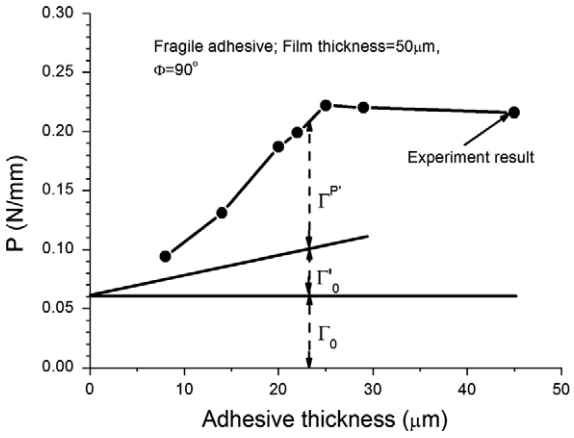

Fig. 12. An estimation for the energy dissipation due to the adhesive layer.

beam bend model and using the 2D FE model respectively, he will obtain the very different interfacial energy Γ_0 based on both analytical models. Since the length scale R_0 (see Eq. (3)) in the analytical results is proportional to Γ_0, while Γ_0 is proportional to the size of the fracture process zone, therefore, relative to the 2D FE model, the beam bend model is suitable for a peeling case with a longer fracture process zone, $L_2^{\mathrm{P}} \gg L_1^{\mathrm{P}}$, where $(L_1^{\mathrm{P}}, L_2^{\mathrm{P}})$ are sizes of fracture process zones based on the 2D FE model and on the bending model, respectively. So one can use the bending model to describe a macroscale peeling process, and use the 2D FE model to describe a small scale peeling process. Additionally, one expects that a microscale peeling process should be described based on the strain gradient plasticity models (Wei and Hutchinson, 1997a; Wei et al., 2004). Summarizing the effectiveness of above several analytical models is sketched in Fig. 13(a) and (b).

4.3. On curvature characterization of peel test

Besides the above analytical criteria, sometime the film curvature at crack tip k_{tip} is taken as a criterion parameter(Cotterell et al., 2006; Zhao and Wei, 2007). The corresponding two-parameter criterion is $(\Gamma_0, k_{\mathrm{tip}})$. Actually, the criterion $(\Gamma_0, k_{\mathrm{tip}})$ is the same one with the criterion $(\Gamma_0, \bar{\varepsilon}_{\mathrm{c}})$, see Fig. 14, since that

$$\bar{\varepsilon}_{\mathrm{c}} = \frac{\sqrt{1-\nu+\nu^2}}{3(1-\nu)} t k_{\mathrm{tip}} \tag{8}$$

for beam bend model (see Eqs. (14), (16) in Wei (2004)). Introducing the elastic limit curvature k_{e} here, from Eq. (8) we have

$$\frac{\bar{\varepsilon}_{\mathrm{c}}}{\varepsilon_{\mathrm{Y}}} = \frac{2}{3}(1+\nu)\frac{k_{\mathrm{tip}}}{k_{\mathrm{e}}} \tag{9}$$

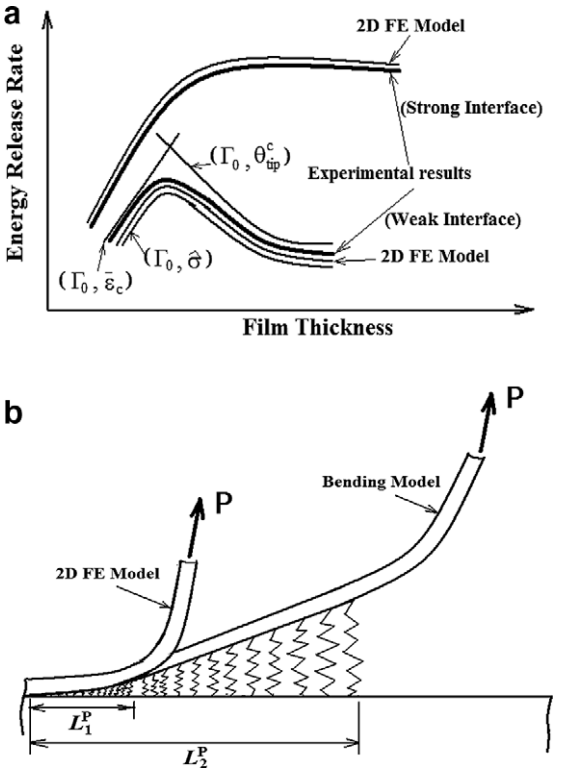

Fig. 13. Checking the effectiveness of the analytical models through comparing solution trends based on models and based on peeling experiments (a) (sketch figure, referring to Figs. 3, 8, 10) (b) Fracture process zones based on both bending model and 2D FE model are different in scale level.

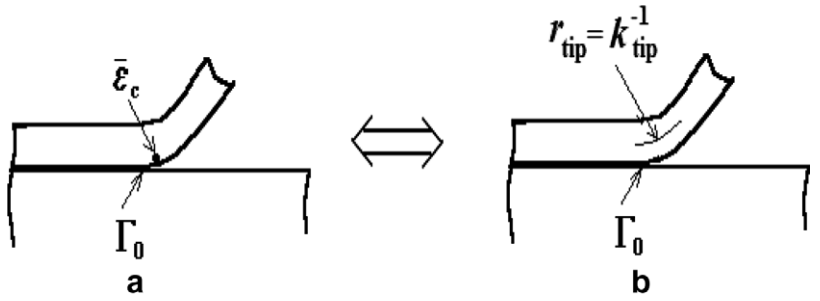

Fig. 14. Sketch figure shows equivalence of the $(\Gamma_0, \bar{\varepsilon}_c)$ criterion with the (Γ_0, k_{tip}) criterion.

where $k_e = 2(1-\nu^2)\sigma_Y/Et\sqrt{1-\nu+\nu^2}$ is the elastic limit curvature. Substituting the expression of $\bar{\varepsilon}_c/\varepsilon_Y$ (Eq. (9)) into the results shown in Fig. 3(a) for $(\Gamma_0, \bar{\varepsilon}_c)$ criterion results, one can easily obtain the results corresponding to the criterion (Γ_0, k_{tip}).

5. Concluding remarks

In the present research, two types of the peeling experiments have been performed. One type of the experiments is for a series of Al film thickness from 20 microns to two hundred microns bonded onto ceramic substrates using an adhesive layer. Another type of the peeling experiments is for several thicknesses of the superthin Cu film electroplated onto the ceramic substrate without adhesive layer. From the peeling experiments, steady-state energy release rates are recorded as the functions of the film thickness. Through comparison of these experimental results with modeling results, effectiveness of the analytical models describing the peel tests can be assessed. Several fundamental and important conclusions are obtained as follows:

1. Cohesive zone criterion based on the beam bend model is suitable for describing a peeling process of a weak interface strength case, and corresponds to much longer size of interface fracture process zone compared with the 2D FE model, while the 2D FE model is suitable for the general case from weak to strong interfaces.
2. Peel test problem of a film/substrate system with an adhesive layer between film and substrate can be equivalently treated with another peel test problem of a film/substrate without adhesive layer. The dissipation energy due to the adhesive layer and the cohesive energy along the adhesive layer can be equivalent to a new cohesive zone model.
3. Criterion $(\Gamma_0, \bar{\varepsilon}_c)$ based on the beam bend model is suitable for a small film thickness case, and it is similar to the criterion (Γ_0, k_{tip}).

It is worth pointing out that in the present analyses, the effect of the residual stress within the film layer has not been considered, and this effect may be important to the ductile film delaminating along ceramic substrate, especially for the case of the high temperature environment. Moreover, through the present investigation for the peel test description, an effective analytical model which is suitable for a general case from weak to strong interface adhesions is still lacking, and needs to be explored in the future studies.

Acknowledgments

This work is supported by the National Science Foundation of China through Grants 10432050, 10428207 and 10672163, by the Chinese Academy of Sciences through Grant KJCX2-YW-M04, and by NSFC through Innovation Team Project (10721202).

References

Andersson, T., Biel, A., 2006. On the effective constitutive properties of a thin adhesive layer loaded in peel. Int. J. Fracture 141 (1-2), 227–246.

Asai, H., Iwase, N., Suga, T., 2001. Influence of ceramic surface treatment on peel-off strength between aluminum nitride and epoxy-modified polyaminobismaleimide adhesive. IEEE Trans. Adv. Pack. 24, 104–112.

Betegon, C., Hancock, J.W., 1991. Two-parameter characterization of elastic–plastic crack-tip fields. J. Appl. Mech. 113, 104–110.

Bundy, K., Schlegel, U., Rahn, B., Geret, V., Perren, S., 2000. Improved peel test method for measurement of adhesion to biomaterials. J. Mater. Sci.: Mater. Med. 11, 517–521.

Choi, J.W., Oh, T.S., 2001. Peel strength and peel angle measured by the T-peel test on Cr/BPDA-PDA interface. J. Adhe. Sci. Tech. 15, 139–152.

Cotterell, B., Hbaieb, K., Williams, J.G., Hadavinia, H., Tropsa, V., 2006. The root rotation in double cantilever beam and peel tests. Mech. Mater. 38 (7), 571–584.

Cotterell, B., Williams, G., Hutchinson, J., Thouless, M., 2002. Annoucement of a round robin on the analysis of the peel test. Int. J. Fracture 114, L9–L13, 2003, 119, L55-L59..

Fedorov, A., De Hosson, J.T.M., 2005. Adhesion of polymer coatings studied by laser-induced delamination, J. Appl. Phys. 97 (12). Art. No. 123510.

Feliu-Baez, R., Lockhart, H.E., Burgess, G., 2001. Correlation of peel and burst tests for pouches. Packaging Tech. Sci. 14, 63–69.

Johnson, K.L., Kauzarich, J.J., 2004. Transfer of adhesive tape between calender rolls. J. Phys. D-Appl. Phys. 37 (5), 774–783, MAR 7 2004.

Kawabe, M., Tasaka, S., Inagaki, N., 2000. Effects of surface modification by oxygen plasma on peel adhesion of pressure-sensitive adhesive tapes. J. Appl. Polym. Sci. 78, 1392–1401.

Kawashita, L.F., Moore, D.R., Williams, J.G., 2005. The measurement of cohesive and interfacial toughness for bonded metal joints with epoxy adhesives. Comp. Interfaces 12 (8-9), 837–852.

Kim, J., Kim, K.S., Kim, Y.H., 1989. Mechanical effects of peel adhesion test. J. Adhe. Sci. Tech. 3, 175–187.

Kim, K.S., Aravas, N., 1988. Elasto-plastic analysis of the peel test. Int. J. Solids Struct. 24, 417–435.

Kim, K.S., Kim, J., 1988. Elasto-plastic analysis of the peel test for thin film adhesion. J. Engin. Mat. Tech. 110, 266–273.

Kinloch, A.J., Lau, C.C., Williams, J.G., 1994. The peeling of flexible laminates. Int. J. Fracture 66, 45–70.

Leseman, Z.C., Carlson, S.P., Mackin, T.J., 2007. Experimental measurements of the strain energy release rate for stiction-failed microcantilevers using a single-cantilever beam peel test. J. Microelectromech. Syst. 16 (1), 38–43.

Moidu, A.K., Sinclair, A.N., Spelt, J.K., 1998. On determination of fracture energy using the peel test. J. Testing Evalu. 26, 247–254.

Moody, N.R., Adams, D.P., Medlin, D., Headley, T., Yang, N., Volinsky, A., 2003. Effects of diffusion on interfacial fracture of gold-chromium hybrid microcircuit films. Int. J. Fracture 119 (4-2), 407–419.

Pardoen, T., Ferracin, T., Landis, C.M., Delannay, F., 2005. Constraint effects in adhesive joint fracture. J. Mech. Phys. Solids 53 (9), 1951–1983.

Park, I.S., Yu, J., 1998. An X-ray study on the mechanical effects of the peel test in a Cu/Cr/polyimide system. Acta Mater. 46, 2947–2953.

Rice, J.R., 1974. Limitations to the small scale yielding approximation for crack tip plasticity. J. Mech. Phys. Solids 22, 17–26.

Spies, G.J., 1953. The peeling test on redux-bonded joints. J. Aircraft Eng. 25, 64–70.

Suo, Z., Shih, C.F., Varias, A.G., 1993. A theory for cleavage cracking in the presence of plastic flow. Acta Metall. Mater. 41, 151–157.

Thouless, M.D., Kafkalidis, M.S., Ward, S.M., et al., 1997. Toughness of plastically-deforming asymmetric joints. Scripta Mater. 37, 1081–1087.

Tvergaard, V., Hutchinson, J.W., 1993. The influence of plasticity on mixed mode interface toughness. J. Mech. Phys. Solids 41, 1119–1135.

Wei, Y., 2002. Thin layer splitting along the elastic–plastic solid surface. Int. J. Fracture 113, 233–252.

Wei, Y., 2004. Modeling nonlinear peeling of ductile thin films—Critical assessment of analytical bending models using FE simulations. Int. J. Solids Struct. 41, 5087–5104.

Wei, Y., Hutchinson, J.W., 1997a. Steady-state crack growth and work of fracture for solids characterized by strain gradient plasticity. J. Mech. Phys. Solids 45, 1253–1273.

Wei, Y., Hutchinson, J.W., 1997b. Nonlinear delamination mechanics for thin films. J. Mech. Phys. Solids 45, 1137–1159.

Wei, Y., Hutchinson, J.W., 1998. Interface strength, work of adhesion and plasticity in the peel test. Int. J. Fracture 93, 315–333.

Wei, Y., Qiu, X., Hwang, K.C., 2004. Steady-state crack growth and fracture work based on the theory of mechanism-based strain gradient plasticity. Eng. Fracture Mech. 71, 107–125.

Wei, Y., Wang, T.C., 1995a. Fracture criterion based on the higher-order asymptotic fields. Int. J. Fracture 73, 39–50.

Wei, Y., Wang, T.C., 1995b. Characterization of elastic–plastic fields near stationary crack tip and fracture criterion. Eng. Fracture Mech. 51, 547–553.

Wei, Y., Zhao, M., Tang, S., 2002. Characterization of the fracture work for ductile film undergoing the micro-scrach. Acta Mech. Sinica 18, 494–505.

Williams, J.A., Kauzlarich, J.J., 2006. Energy and force distributions during mandrel peeling of a flexible tape with a pressure-sensitive adhesive. J. Adhes. Sci. Tech. 20 (7), 661–676.

Williams, J.A., Kauzlarich, J.J., 2005. The influence of peel angle on the mechanics of peeling flexible adherends with arbitrary load-extension characteristics. Tribol. Intl. 38 (11-12), 951–958.

Yang, Q.D., Thouless, M.D., Word, S.M., 1999. Numerical simulations of adhesively-bonded beams failing with extensive plastic deformation. J. Mech. Phys. Solids 47, 1337–1353.

Zhao, H., Wei, Y., 2007. Determination of interface properties between micron-thick metal film and ceramic substrate using peel test. Int. J. Fracture 144, 103–112.

Zhao, H., 2007. Experiments and numerical simulations of peel test, PhD thesis of the Graduate School, Chinese Academy of Sciences, Page 53 (In Chinese).